













# De Novo Missense Variants in *SLC32A1* Cause a Developmental and Epileptic Encephalopathy Due to Impaired GABAergic Neurotransmission

Konrad Platzer, MD <sup>1</sup>, Heinrich Sticht, PhD <sup>2</sup>, Caleb Bupp, MD <sup>3</sup>,  
Mythily Ganapathi, PhD <sup>4</sup>, Elaine M. Pereira, MD <sup>5</sup>, Gwenaël Le Guyader, MD <sup>6</sup>,  
Frederic Bilan, PhD <sup>6,7</sup>, Lindsay B. Henderson, PhD <sup>8</sup>, Johannes R. Lemke, MD <sup>1,9</sup>,  
Holger Taschenberger, PhD <sup>10</sup>, Nils Brose, PhD <sup>10</sup>, Rami Abou Jamra, MD <sup>1†</sup> and  
Sonja M. Wojcik, PhD <sup>10†</sup>

**Objective:** Rare inherited missense variants in *SLC32A1*, the gene that encodes the vesicular gamma-aminobutyric acid (GABA) transporter, have recently been shown to cause genetic epilepsy with febrile seizures plus. We aimed to clarify if de novo missense variants in *SLC32A1* can also cause epilepsy with impaired neurodevelopment.

**Methods:** Using exome sequencing, we identified four individuals with a developmental and epileptic encephalopathy and de novo missense variants in *SLC32A1*. To assess causality, we performed functional evaluation of the identified variants in a murine neuronal cell culture model.

**Results:** The main phenotype comprises moderate-to-severe intellectual disability, infantile-onset epilepsy within the first 18 months of life, and a choreiform, dystonic, or dyskinetic movement disorder. In silico modeling and functional analyses reveal that three of these variants, which are located in helices that line the putative GABA transport pathway, result in reduced quantal size, consistent with impaired filling of synaptic vesicles with GABA. The fourth variant, located in the vesicular gamma-aminobutyric acid N-terminus, does not affect quantal size, but increases presynaptic release probability, leading to more severe synaptic depression during high-frequency stimulation. Thus, variants in vesicular gamma-aminobutyric acid can impair GABAergic neurotransmission through at least two mechanisms, by affecting synaptic vesicle filling and by altering synaptic short-term plasticity.

**Interpretation:** This work establishes de novo missense variants in *SLC32A1* as a novel cause of a developmental and epileptic encephalopathy.

## Summary for Social Media If Published:

View this article online at [wileyonlinelibrary.com](https://onlinelibrary.wiley.com/doi/10.1002/ana.26485). DOI: 10.1002/ana.26485

Received Apr 1, 2022, and in revised form Aug 16, 2022. Accepted for publication Aug 17, 2022.

Address correspondence to Dr Platzer, Institute of Human Genetics, University of Leipzig Medical Center, Leipzig, Germany and Dr Wojcik, Department of Molecular Neurobiology, Max Planck Institute for Multidisciplinary Sciences, Göttingen, Germany. E-mail: [konrad.platzer@medizin.uni-leipzig.de](mailto:konrad.platzer@medizin.uni-leipzig.de). Dr Sonja M. Wojcik, Department of Molecular Neurobiology, Max Planck Institute for Multidisciplinary Sciences, Göttingen, Germany. E-mail: [wojcik@mpinat.mpg.de](mailto:wojcik@mpinat.mpg.de)

<sup>†</sup>These authors contributed equally to this work.

From the <sup>1</sup>Institute of Human Genetics, University of Leipzig Medical Center, Leipzig, Germany; <sup>2</sup>Institute of Biochemistry, Friedrich-Alexander University Erlangen-Nürnberg, Erlangen, Germany; <sup>3</sup>Spectrum Health Medical Genetics, Grand Rapids, Michigan; <sup>4</sup>Department of Pathology and Cell Biology, Columbia University Medical Center, New York, New York; <sup>5</sup>Department of Pediatrics, Columbia University Irving Medical Center, New York, New York; <sup>6</sup>Department of Genetics, Poitiers University Hospital Center, Poitiers Cedex, France; <sup>7</sup>Laboratory of Experimental and Clinical Neurosciences (LNEC) INSERM U1084, University of Poitiers, Poitiers, France; <sup>8</sup>GeneDx, Gaithersburg, Maryland; <sup>9</sup>Center for Rare Diseases, University of Leipzig Medical Center, Leipzig, Germany; and <sup>10</sup>Department of Molecular Neurobiology, Max Planck Institute for Multidisciplinary Sciences, Göttingen, Germany

Additional supporting information can be found in the online version of this article.

958 © 2022 The Authors. *Annals of Neurology* published by Wiley Periodicals LLC on behalf of American Neurological Association. This is an open access article under the terms of the [Creative Commons Attribution-NonCommercial-NoDerivs](https://creativecommons.org/licenses/by-nc-nd/4.0/) License, which permits use and distribution in any medium, provided the original work is properly cited, the use is non-commercial and no modifications or adaptations are made.

1. @platzer\_k @lemke\_johannes @RamiJamra @Nirgalito @GeneDx
2. The SLC family 32 Member 1 (SLC32A1) is the only protein identified to date, that loads gamma-aminobutyric acid (GABA) and glycine into synaptic vesicles, and is therefore also known as the vesicular GABA transporter (VGAT) or vesicular inhibitory amino acid transporter (VIAAT). Rare inherited missense variants in SLC32A1, the gene that encodes VGAT/vesicular inhibitory amino acid transporter, have recently been shown to cause genetic epilepsy with febrile seizures plus.
3. We aimed to clarify if de novo missense variants in *SLC32A1* can also cause epilepsy with impaired neurodevelopment.
4. We report on four individuals with de novo missense variants in *SLC32A1* and a developmental and epileptic encephalopathy with infantile onset epilepsy. We establish causality of the variants via in silico modeling and their functional evaluation in a murine neuronal cell culture model.
5. *SLC32A1* variants represent a novel genetic etiology in neurodevelopmental disorders with epilepsy and a new GABA-related disease mechanism.

ANN NEUROL 2022;92:958–973

## Abbreviations

AP	action potential
DD	developmental delay
DEE	developmental and epileptic encephalopathy
DIV	day <i>in vitro</i>
GEFS+	genetic epilepsy with febrile seizures plus
Het	heterozygous
ID	intellectual disability
IPSC	inhibitory postsynaptic current
KO	knockout
mIPSC	miniature Inhibitory Postsynaptic Current
SV	synaptic vesicle
VGAT	vesicular GABA transporter
VIAAT	vesicular inhibitory amino acid transporter
WT	wild type

## Introduction

Members of the solute carrier (SLC) protein family transport a wide range of substrates, with amino acids being the most frequent.<sup>1</sup> The SLC family 32 member 1 (SLC32A1) is the only protein identified to date that loads gamma-aminobutyric acid (GABA) and glycine into synaptic vesicles (SVs), and is therefore also known as the vesicular GABA transporter (VGAT) or vesicular inhibitory amino acid transporter (VIAAT). Although GABA is an important inhibitory neurotransmitter crucial for the proper function of the mature brain, both GABA and glycine act as inhibitory neurotransmitters in the spinal cord and brainstem. Homozygous *Slc32a1* knockout mice (*Slc32a1*<sup>KO</sup>) are embryonically lethal,<sup>2</sup> whereas heterozygotes show no abnormalities in behavioral assays.<sup>3</sup> As disruption of GABAergic neurotransmission is an established cause of epilepsy and neurodevelopmental disorders,<sup>4</sup> impaired VGAT function constitutes a plausible cause for a developmental and epileptic encephalopathy. Rare heterozygous missense variants in *SLC32A1* have recently been described to segregate in families with a phenotype

of genetic epilepsy with febrile seizures plus (GEFS+) and idiopathic generalized epilepsy.<sup>5</sup> Affected family members showed a wide range of seizure types; for example, febrile seizures, focal seizures, generalized seizures, and unclassified seizures, but no developmental delay (DD) or intellectual disability (ID).

In this study, we report on four individuals with de novo missense variants in *SLC32A1*, and a developmental and epileptic encephalopathy with infantile onset epilepsy. We establish causality of the variants through in silico modeling and their functional evaluation in a murine neuronal cell culture model.

## Subjects and Methods

### Study Subjects and Study Approval

This study was approved by the ethics committee of the University of Leipzig (402/16-ek). With the help of GeneMatcher<sup>6</sup> we identified four individuals harboring heterozygous de novo missense variants in *SLC32A1* with an overlapping phenotype of a developmental and epileptic encephalopathy with DD/ID and early-onset epilepsy at different centers in Germany, France, and the USA. The collaborating physicians provided detailed clinical information through a uniform clinical questionnaire (Supplemental Table 1). Informed consent was obtained from all examined individuals or their legal guardians. For some cases, testing was carried out as part of routine clinical care, and therefore institutional ethics approval was not required. If done in a research setting, the testing was approved by the ethics committees of the respective centers. All families provided informed consent to clinical testing and publication.

### Identification and Evaluation of Variants

Exome sequencing using standard commercial products within diagnostic or research settings was performed in all four families. As no causative variant was identified in a known disease gene in any of the four index individuals, evaluation of the exome sequencing data was performed to potentially identify variants in candidate genes. To prioritize variants in known disease, as well as candidate genes, the following aspects were considered: gene and variant attributes, a minor allele frequency of below 1% in

the general population, assumed effect on protein function, in silico prediction tools, phenotype, family history, and inheritance according to the local proceedings in the respective centers. De novo occurrence of the variants in *SLC32A1* was confirmed in all individuals. For in silico prediction of missense variants, the following tools were used: CADD, REVEL, MutationTaster, M-CAP, PolyPhen-2, and GERP++.<sup>7–12</sup> Families of individuals 1–3 underwent trio exome sequencing. Clinical trio exome sequencing was performed for individual 3, as previously described,<sup>13</sup> and subsequently confirmed with Sanger sequencing. The de novo variant in individual 4 was identified by singleton exome sequencing and subsequent validation of de novo occurrence with Sanger sequencing. The databases of the Genome Aggregation Database (gnomAD, v2.1.1) served as control populations.<sup>14</sup>

### Structural Modeling

The structure of VGAT was modeled with HHpred<sup>15</sup> and Modeller<sup>16</sup> using the crystal structure of the transporter SLC38A9 (PDB: 6C08<sup>17</sup>) as a template. The arginine substrate present in the template structure was replaced by GABA. The effect of the sequence variants was investigated with the tools VIPUR<sup>18</sup> and Missense3D.<sup>19</sup> VMD<sup>20</sup> and RasMol<sup>21</sup> were used for structure analysis and visualization.

### Lentiviral Constructs

Murine VGAT cDNA was amplified from a C57Bl/6N cDNA library using the primers 5'-CGGCTAGCGCGAGG GTCATGAGCCAGAGC-3' and 5'-GCTTCGAATGGGGG TGGGGGCGGGAATGAC-3'. PCR products were subcloned into the pCR<sup>TM</sup>II-TOPO vector (ThermoFisher, Waltham, MA, USA). Each variant was then introduced using QuikChange mutagenesis (Agilent, Santa Clara, CA, USA). WT and the four mutated VGAT cDNAs were then subcloned using the primer-derived NheI and BstBI sites into a lentiviral vector, which expresses the target gene under control of a Synapsin-1 promoter and an EGFP reporter from a separate ubiquitin C promoter.<sup>22</sup> Lentiviral particles were produced according to published protocols.<sup>23,24</sup>

### Neuron Culture and Electrophysiological Recordings

Autaptic microisland cultures of striatal neurons were prepared from embryonic day (E)17.5 mouse embryos, as previously described.<sup>2,25,26</sup> Cultures were infected with lentiviral particles on day *in vitro* (DIV) 2–3 and patch-clamp recordings were performed between DIV 9–14. Whole-cell voltage clamp recordings were acquired at room temperature (22°C–25°C) using an EPC-10 amplifier and Patchmaster software (HEKA, Lambrecht, Germany). Whole-cell capacitance was estimated from capacitive current transients in response to 10-mV step depolarizations assuming a simple two-compartment model.<sup>27</sup> Capacitance values reported in Tables 3 and 4 represent total cell capacitance; that is, the sum of  $C_1$  (representing soma and proximal dendrites) and  $C_2$  (representing distal dendrites) of the two-compartment equivalent circuit model of Mennerick et al.<sup>27</sup> The

intracellular solution contained (in mM) 100 KCl, 40 K-Gluconate, 10 HEPES, 0.1 EGTA, 4 MgATP, 0.3 Na<sub>2</sub>GTP, 15 creatine phosphate, and 5 U/ml phosphocreatine kinase (315 mOsm/l, pH 7.2). The standard extracellular solution contained (in mM) 140 NaCl, 2.4 KCl, 10 HEPES, 10 glucose, 2 CaCl<sub>2</sub>, and 4 MgCl<sub>2</sub> (305–307 mOsm/l, pH 7.4). For estimating current responses elicited by hyperosmotic stimulation ( $I_{\text{sucrose}}$ ), the standard bath solution was supplemented with 500 mM sucrose and CaCl<sub>2</sub> was omitted. A custom-made fast-flow perfusion system consisting of glass capillaries controlled by a stepper motor, which allows a complete solution exchange around the recorded neuron, was used to rapidly switch between extracellular solutions. Inhibitory postsynaptic currents (IPSCs) were evoked by depolarizing voltage steps of 1-ms duration from the holding potential of –70 mV to –20 mV. Liquid junction potentials were not corrected for. The GABAergic nature of postsynaptic currents was confirmed by their sensitivity to 20  $\mu$ M (–)-bicuculline methiodide (Hello Bio, Princeton, NJ, USA). Single action potential (AP)-evoked IPSCs were recorded at an interstimulus interval of 10 s, which was sufficiently long enough to allow for full recovery from synaptic depression, and 10–15 IPSCs were averaged for analysis. Trains of IPSCs, evoked by stimulus trains of 30 and 40 stimuli, delivered at frequencies of 10 Hz and 40 Hz, respectively, were recorded three times for each cell, with 1.5-minute intervals in between successive trials, and averaged before analysis. As miniature inhibitory postsynaptic current (mIPSC) frequency was found to be low in resting autaptic striatal neurons, mIPSCs were recorded after each 10-Hz train for 1.5 minutes, for a total duration of 4.5 minutes. For mIPSC recordings under conditions of elevated osmolarity (355–357 mOsm/l), 50 mM sucrose were added to the standard extracellular solution. Spontaneously occurring mIPSCs were detected in continuous recordings by a template matching algorithm<sup>28</sup> implemented in Igor Pro (Wavemetrics, Portland, OR, USA). Analyses were performed using Igor Pro and Prism (GraphPad, San Diego, CA, USA).

### Western Blot Analysis

Western blotting was carried out on striatal mass cultures, which were prepared according to the same protocols as autaptic cultures,<sup>2,25</sup> but plated on poly-L-lysine at a density of 7,000 cells/cm<sup>2</sup> and kept in Dulbecco's Modified Eagle's Medium with GlutaMAX<sup>TM</sup> (Gibco, Waltham, MA, UAA; 31966–021) with 10% fetal bovine serum and B27-supplement (Gibco; 17504–044) for DIV 1. Cultures were infected on DIV 2 and harvested on DIV 9. Primary antibodies used for western blots were mouse-anti-synapsin (Synaptic Systems, Göttingen, Germany; 106,011) at 1:6,000, rabbit-anti-VGAT (Synaptic Systems, 131,013) at 1:1,000, and mouse-anti-EGFP (Roche, 11,814,460,001) at 1:3,000. Secondary antibodies used were horseradish peroxidase coupled goat-anti-mouse (Jackson ImmunoResearch, West Grove, PA, USA; 115-035-146) at 1:10,000 and goat-anti-rabbit (Jackson ImmunoResearch; 111-035-144) at 1:10,000. Enhanced chemiluminescence (Amersham, Amersham, UK; RPN3004) was documented using an Intas ECL Chemostar Plus Imager (Intas, Göttingen, Germany).

## Statistics

Electrophysiological data are presented as the mean  $\pm$  standard error of the mean. Statistical significance was assessed using Kruskal–Wallis with post-hoc Dunn's correction for multiple comparisons. To obtain estimates for the mean vesicular release probability  $\bar{p}_{vr}$  from IPSC versus  $I_{sucrose}$  scatter plots (Fig. 2F, Fig. 4F, Tables 3, and 4), the matrix consisting of  $IPSC^{i,gt}$  and  $I_{sucrose}^{i,gt}$ , where  $i$  and  $gt$  denote cell index and genotype, respectively, was fitted with a linear model (intercept forced to zero) using R (The R Foundation for Statistical Computing, Vienna, Austria), with  $I_{sucrose}$  being the predictor variable and  $gt$  the interaction term, and statistical significance values ( $p$  value) were adjusted for multiple comparisons using Tukey's method (R package 'emmeans'). Standard error of the mean estimates for release probabilities  $p_{EQ}$  derived from line fits to Elmqvist–Quastel plots (Fig. 3H) were obtained by bootstrap resampling analysis using a balanced bootstrap approach implemented in Igor Pro (every experimental observation appeared exactly the same number of times in the total population of 2,000 bootstrap samples),<sup>29,30</sup> and statistical significance values ( $p$  values) were adjusted for multiple comparisons using Bonferroni's method.

## Results

### Clinical Description

Detailed clinical data on all four individuals are presented in Table 1, Table 2, in the Supplemental case reports, and Supplemental Table 1. All four individuals showed global developmental delay and moderate-to-severe intellectual disability. Seizure onset was in the neonatal period in individuals 1 and 4 (at age 4 months and 1 month, respectively), and in early infancy in individuals 2 and 3 (at age 15 months and 18 months, respectively). Individuals 1 and 4 presented initially with focal and focal impaired awareness seizures, whereas in individuals 2 and 3 generalized tonic–clonic seizures predominated. In addition, individual 2 showed myoclonic seizures and status epilepticus with suspicion of myoclonic atonic epilepsy. She also showed focal impaired awareness seizures. Despite the initial focal seizure semiology of individual 4, this individual later developed generalized epilepsy with generalized atonic, myoclonic, and generalized tonic–clonic seizures, as well as eyelid myoclonia. The initial seizure semiology

**TABLE 1. Summary of Clinical Symptoms of Individuals with De Novo Variants in SLC32A1**

Individual	1	2	3	4
<b>Variant (NM_080552.3)</b>	c.271G > A, p. (Ala91Thr), de novo	c.787G > A, p. (Val263Met), de novo	c.806 T > C, p. (Leu269Pro), de novo	c.965 T > G, p. (Phe322Cys), de novo
<b>Sex, age at last assessment</b>	M, 6 y 3 m	F, 5 y 4 m	M, 10 y 1 m	F, 6 y 9 m
<b>DD/ID, severity</b>	Yes, severe, nonverbal	Yes, moderate	Yes, not assessed	Yes, severe, nonverbal
<b>Developmental course with periods of slowing or regression</b>	At age ca. 8 months he regressed when he lost the ability to roll over.	Multiple episodes of regression at around age 2 years 7 months during increased seizure frequency: she lost the ability to sit, walk, speak & eat independently. Skills were repeatedly regained after better seizure control.	When he was 3 years old, he began to have falling episodes. By age 6 years he was having difficulties with reading & writing. As he has gotten older, his speech has gotten worse. He needed to repeat 1st grade & was placed in special education.	Epilepsy was generally well controlled until age 5 years when she lost the ability to walk. Change of treatment controlled seizures & she showed improved interactions & started playing again.
<b>Movement disorder</b>	No	Intermittent choreiform-like, dystonic	Choreiform	Paroxysmal dyskinesia
<b>MRI</b>	ventriculomegaly, loss of white matter, thinning of the corpus callosum	cerebral atrophy	Normal	Normal

Further clinical details are provided in Table S1.  
DD = developmental delay; F = female; ID = intellectual disability; M = male; MRI = magnetic resonance imaging.

**TABLE 2. Summary of epilepsy and electroencephalogram findings of individuals with *de novo* variants in SLC32A1. Further clinical details are provided in Table S1**

Individual	1	2	3	4
<b>Seizures, onset</b>	Yes, 4 m	Yes, 1 y 3 m	Yes, 1 y 6 m	Yes, 1 m
<b>Seizure types</b>	focal impaired awareness seizures	myoclonic seizures, atonic seizures, generalized tonic-clonic, focal impaired awareness seizures, atypical absence	tonic-clonic	focal & focal impaired awareness seizures, atonic, myoclonic, tonic-clonic
<b>EEG findings</b>	EEG at onset was normal. Follow up at age 2 years: epileptiform discharges in left parietal & right temporal regions. At age 2 years 11 months: rudimentary posterior dominant rhythm; diffuse generalized slowing; reversal anterior/posterior gradient; rudimentary sleep architecture & multifocal epileptiform discharges mainly seen in posterior quadrants & mid temporal regions bilaterally.	Initially: sharp-wave paroxysmal Follow-up: multifocal changes described as “hypsarrhythmia-like” Further follow-up: severe slowing & generalized polyspikes & polyspike wave complexes;	At age 6 years: presence of focal slowing over occipital regions; no epileptiform discharges. Follow up at age 8 years with bursts of generalized spikes & polyspikes on 2 occasions 50-75uV amplitude, lasting for 0.5–1 second only. At last follow up: generalized spikes & polyspikes in sleep & bursts of generalized spikes & polyspikes on 2 occasions 50-75uV amplitude, lasting for 0.5–1 second only	First EEG was performed at 3 weeks of life: many peaks & slow peaks with sometimes an aspect of fast rhythms. One crisis was recorded where we see a discharge of spikes & slow spikes at the level of the right cerebral hemisphere then a passage of spikes is observed with a discharge of rhythmic spikes at the level of the left hemisphere
<b>Epilepsy disorder</b>	Focal epilepsy with impaired awareness	Multifocal epilepsy/ Lennox–Gastaut syndrome	Generalized epilepsy	Focal & generalized epilepsy
<b>Fever as a trigger for seizures</b>	No	Yes	Yes	No

EEG = electroencephalogram.

corresponded to the electroencephalogram pattern, which showed focal epileptiform discharges in individual 1 (on the right and left hemisphere) and individual 4 (slow spikes on the right hemisphere followed by rhythmic discharges on the left). In individual 2, a multifocal pattern was seen on electroencephalogram (described as “hypsarrhythmia-like”), which evolved into severe slowing and generalized polyspikes, and polyspike-wave complexes. In individual 3, generalized spikes and polyspikes were seen on electroencephalogram. During the course of epilepsy, all four individuals experienced at least some long-lasting periods of seizure freedom. Individuals 2, 3, and 4 showed choreiform, choreiform-like, dystonic, or

dyskinetic movement phenotypes, which in individual 3 did not show substantial improvement upon therapy with valproate. In times when seizures intensified, all individuals had periods of developmental slowing and also regression: at approximately 8 months of age, individual 1 regressed when he lost the ability to roll over. Individual 2 showed repeated periods of regression, starting at the age of 2 years and 7 months. With the help of adapted anticonvulsive therapy and improved seizure control, she regained skills, such as her motor abilities to sit, to eat independently, and to speak, although speech was often slurred. Speech slurring then improved over time. Individual 3, when he was aged 3 years, began to have falling

**TABLE 3. Characteristics of GABAergic synaptic transmission: vesicular gamma-aminobutyric acid transporter variants in *Slc32a1*<sup>KO</sup> background**

	VGAT <sup>WT</sup> in KO	VGAT <sup>A90T</sup> in KO	VGAT <sup>V263M</sup> in KO	VGAT <sup>L269P</sup> in KO	VGAT <sup>F322C</sup> in KO
Cell Capacitance (pF)	23.41 ± 1.04 n = 64	24.67 ± 1.28 n = 28	24.12 ± 1.36 n = 35	21.16 ± 1.25 n = 24	24.64 ± 2.22 n = 35
Initial IPSC Amplitude (nA) (Fig. 2B)	2.12 ± 0.21 n = 64	2.96 ± 0.46 n = 28	1.12 ± 0.2 n = 38 **	0.98 ± 0.19 n = 24 **	0.84 ± 0.18 n = 35 ****
Initial IPSC Charge (pC) (Fig. 2C)	79.13 ± 8.08 n = 64	117.4 ± 18.64 n = 27	36.32 ± 7.82 n = 37 ***	37.01 ± 7.12 n = 25 **	31.54 ± 8.047 n = 31 ****
I <sub>Sucrose</sub> Charge (pC)	652.2 ± 54.8 n = 62	804 ± 102.1 n = 24	333.9 ± 54.0 n = 35 ***	338.5 ± 55.6 n = 23 **	306.3 ± 77.4 n = 28 ****
Average Vesicular Release Probability $\bar{P}_{vr}$ (Fig. 2F)	0.111 ± 0.009 n = 62	0.151 ± 0.016 n = 24 *	0.104 ± 0.014 n = 35	0.103 ± 0.013 n = 23	0.108 ± 0.006 n = 28
mIPSC Amplitude (pA) (Fig. 2H)	25.18 ± 1.67 n = 51	29.34 ± 3.38 n = 20	17.53 ± 1.46 n = 33 **	15.61 ± 1.62 n = 20 **	15.55 ± 1.4 n = 23 **
mIPSC Half-Width (ms)	11.19 ± 0.33 n = 51	10.72 ± 0.4 n = 20	10.45 ± 0.29 n = 30	10.83 ± 0.4 n = 20	10.27 ± 0.31 n = 22
mIPSC Frequency (Hz)	1.31 ± 0.2 n = 51	1.16 ± 0.2 n = 20	0.92 ± 0.14 n = 33	0.88 ± 0.27 n = 20	0.52 ± 0.07 n = 23 *
mIPSC Half-Width (ms) at 355 mOsm	11.2 ± 0.35 n = 45	10.96 ± 0.43 n = 18	10.51 ± 0.29 n = 31	10.93 ± 0.49 n = 21	10.11 ± 0.35 n = 25
mIPSC Rise Time (μs) at 355 mOsm	472.4 ± 13.71 n = 45	488.7 ± 30.13 n = 18	552.7 ± 20.17 n = 31 **	565.8 ± 30.91 n = 20 *	572.8 ± 28.95 n = 25 **
mIPSC Decay Time Constant (ms) at 355 mOsm	36.91 ± 1.91 n = 41	33.21 ± 2.76 n = 16	40.41 ± 4.03 n = 22	47.16 ± 6.7 n = 16	37.68 ± 2.94 n = 15
mIPSC Frequency (Hz) at 355 mOsm	1.32 ± 0.18 n = 45	1.24 ± 0.27 n = 18	1.11 ± 0.18 n = 31	0.68 ± 0.09 n = 21	0.65 ± 0.11 n = 25 **
Total Charge 10 Hz Train (nC) (Fig. 3C)	1.19 ± 0.12 n = 54	1.37 ± 0.18 n = 23	0.60 ± 0.1 n = 32 **	0.64 ± 0.16 n = 19 *	0.35 ± 0.09 n = 23 ****
Total Charge 40 Hz Train (nC) (Fig. 3F)	1.05 ± 0.1 n = 48	1.07 ± 0.14 n = 22	0.53 ± 0.09 n = 31 **	0.54 ± 0.14 n = 19 **	0.29 ± 0.09 n = 20 ****
Cumulative Synchronous Charge 40 Hz Train (nC) (Fig. 3G)	0.179	0.175	0.121	0.102	0.077
Release Probability $p_{EQ}$ (Fig. 3H)	0.439 ± 0.034 n = 48	0.587 ± 0.038 n = 22 *	0.330 ± 0.069 n = 31	0.466 ± 0.064 n = 19	0.436 ± 0.08 n = 20

IPSC = inhibitory postsynaptic current; KO = knockout; mIPSC = miniature inhibitory postsynaptic current; VGAT = vesicular gamma-aminobutyric acid transporter.

**TABLE 4. Characteristics of GABAergic synaptic transmission: vesicular gamma-aminobutyric acid transporter variants in *Slc32a1*<sup>WT/Het</sup> background**

	VGAT <sup>WT</sup> in WT/Het	VGAT <sup>A90T</sup> in WT/Het	VGAT <sup>V263M</sup> in WT/Het	VGAT <sup>L269P</sup> in WT/Het	VGAT <sup>F322C</sup> in WT/Het	WT/Het (Ctr n.i.)
Cell Capacitance (pF)	21.2 ± 1.14 n = 36	19.8 ± 1.63 n = 25	24.31 ± 1.34 n = 24	21.86 ± 1.33 n = 26	23.77 ± 1.75 n = 20	27.32 ± 2.17 n = 23
Initial IPSC Amplitude (nA) (Fig. 4B)	3.46 ± 0.44 n = 36	2.28 ± 0.48 n = 24	2.31 ± 0.37 n = 24	2.51 ± 0.35 n = 26	2.93 ± 0.45 n = 20	
Initial IPSC Charge (pC) (Fig. 4C)	140.5 ± 17.9 n = 36	90.39 ± 21.41 n = 24	102 ± 19.04 n = 24	100.5 ± 16.61 n = 26	117 ± 19.56 n = 20	
I <sub>Sucrose</sub> Charge (pC) (Fig. 4E)	880.9 ± 94.6 n = 34	667.5 ± 98.5 n = 24	653.3 ± 84.7 n = 24	725.9 ± 93.6 n = 25	702.1 ± 89.5 n = 19	
Average Vesicular Release Probability $\bar{p}_{vr}$ (Fig. 4F)	0.151 ± 0.015 n = 34	0.138 ± 0.020 n = 24	0.159 ± 0.017 n = 24	0.136 ± 0.015 n = 25	0.162 ± 0.017 n = 19	
mIPSC Amplitude (pA) (Fig. 4H)	33.01 ± 3.23 n = 32	24.54 ± 2.53 n = 23	24.05 ± 3.04 n = 19	23.78 ± 2.28 n = 24	24.66 ± 3.94 n = 13	26.83 ± 1.99 n = 18
mIPSC Half-Width (ms)	10.95 ± 0.39 n = 32	11.29 ± 0.41 n = 23	10.46 ± 0.31 n = 19	10.9 ± 0.31 n = 24	10.79 ± 0.67 n = 13	11.62 ± 0.73 n = 18
mIPSC Rise Time (μs)	432.2 ± 12.5 n = 32	420.3 ± 9.1 n = 23	453.3 ± 25.5 n = 18	464.2 ± 16.0 n = 24	438.4 ± 29.7 n = 13	417.8 ± 22.9 n = 18
mIPSC Frequency (Hz)	1.61 ± 0.36 n = 32	1.06 ± 0.16 n = 23	1.53 ± 0.38 n = 19	1.69 ± 0.27 n = 24	1.08 ± 0.2 n = 13	2.79 ± 0.53 n = 18

Het = heterozygous; IPSC = inhibitory postsynaptic current; mIPSC = miniature inhibitory postsynaptic current; VGAT = vesicular gamma-aminobutyric acid transporter; WT = wild-type.

episodes as his gait worsened. By age 6 years, he had difficulties with reading and writing, and over time, his speech deteriorated. He needed to repeat first grade and was placed in special education. Seizures in individual 4 were generally well controlled until age 5 years, but then she experienced exacerbation of seizures and subsequently lost the ability to walk. A change of treatment reinstated seizure control, and she showed improved interactions and started playing again. Cranial imaging of individuals 3 and 4 showed normal results. The brain magnetic resonance imaging of individual 1 revealed ventriculomegaly, loss of white matter, and thinning of the corpus callosum. In individual 2, cerebral atrophy was noted.

### Causative Variants

All four de novo variants in *SLC32A1* identified in this study comprise missense changes (Fig. 1). All variants are absent from gnomAD. Variants in individuals 2 (p.Val263Met), 3 (p.Leu269Pro), and 4 (p.Phe322Cys)

affect highly conserved amino acids, and are predicted to be damaging by multiple in silico prediction tools (Table S2). All three variants are located in helices that form the substrate transport pathway. The de novo variant in individual 1 (p.Ala91Thr) affects a weakly conserved amino acid and is predicted to be benign by most in silico prediction tools. Individual 1 had a second de novo variant: Chr16(GRCh37):g.1252243, NM\_021098.2: c.1793C > T, p.(Ala598Val) in the *CACNA1H* gene.

### Structural Modeling

A VGAT model, comprising the transmembrane domain (residues 115–509) of the transporter, allowed us to investigate the structural consequences of the variants p.(Val263Met), p.(Leu269Pro), and p.(Phe322Cys) in more detail. All three missense variants are located in helices that line the substrate transport pathway (Fig. 1A,B). A closer view of the VGAT structure, which represents the cytosol-open state of the transporter, revealed that residues

Val263 and Phe322 line a deep cavity with the GABA substrate at its bottom (Fig. 1C). The variants p.(Val263Met) and p.(Phe322Cys) are predicted to cause a significant ( $\geq 70 \text{ \AA}^3$ ) change in the size of this cavity, indicating that they likely affect substrate uptake on the cytosolic side or the transport process itself. The fact that Val263 and Phe322 are accessible from the cytosolic side (Fig. 1C) indicates that mutating these sites might additionally affect binding of cytosolic interaction partners to VGAT. Leu269 is located in an  $\alpha$ -helix that flanks the central cavity. An exchange to proline causes steric interference with the adjacent Leu268 (Fig. 1D), which destabilizes the structure close to the site of substrate transport.

### Functional Analyses

To examine the effects of the four VGAT variants on inhibitory neurotransmission, we expressed lentiviral constructs of each variant in striatal GABAergic mouse neurons in microisland cultures. Single neurons growing on astrocyte microislands only form synapses with themselves. Electrophysiological recordings from such isolated, autaptic neurons allow for the detailed analysis of neurotransmission of individual neurons under defined conditions and are ideally suited for structure–function analyses of synaptic proteins.<sup>2,25,31–33</sup>

Human and murine VGAT show 98.5% identity at the amino acid level. The majority of amino acid exchanges between species can be found in the N-terminal

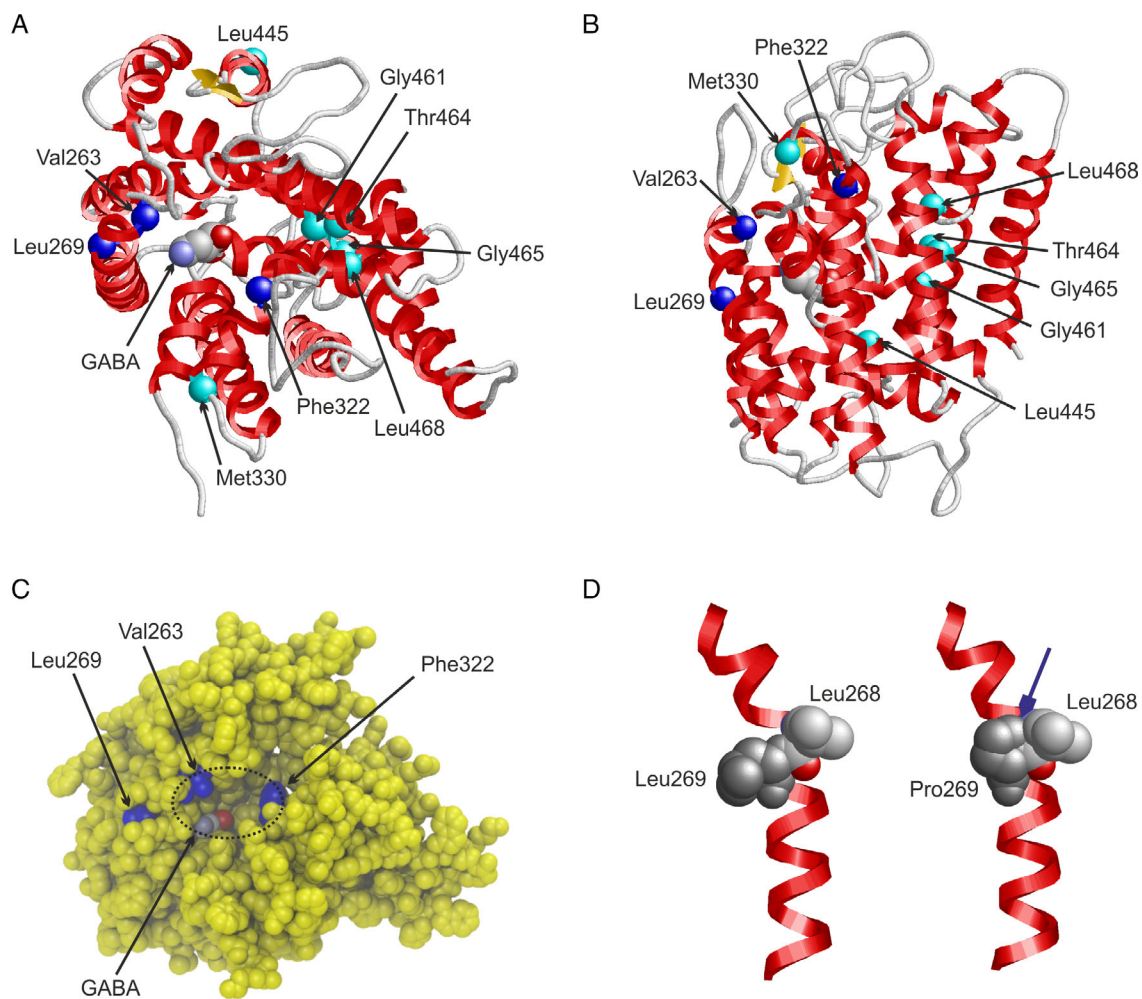


**FIGURE 1:** Model of the vesicular gamma-aminobutyric acid transporter (VGAT) transmembrane domain. (A) View on VGAT from the cytosolic side indicating the sites of sequence variants. Positions described in the present study are highlighted as blue spheres, whereas additional positions identified in the previous study by Heron et al.<sup>5</sup> are marked as cyan spheres. The structure is shown in ribbon presentation with helices highlighted in red and the substrate gamma-aminobutyric acid in space-filled presentation (atom-type coloring). (B) Side view on VGAT, which is rotated by  $90^\circ$  around the horizontal axis compared with the view in A. (C) View from the cytosolic side on VGAT in space-filled presentation (same orientation as in A). The dotted circle marks a cavity that is lined by Val263 and Phe322. The position of a gamma-aminobutyric acid molecule at the bottom of the cavity is also indicated. (D) Leu269 is located in one of the transmembrane helices (left). A proline at this position (right) will cause steric clashes (marked by an arrow) with the adjacent Leu268 thereby affecting the helix conformation and stability.



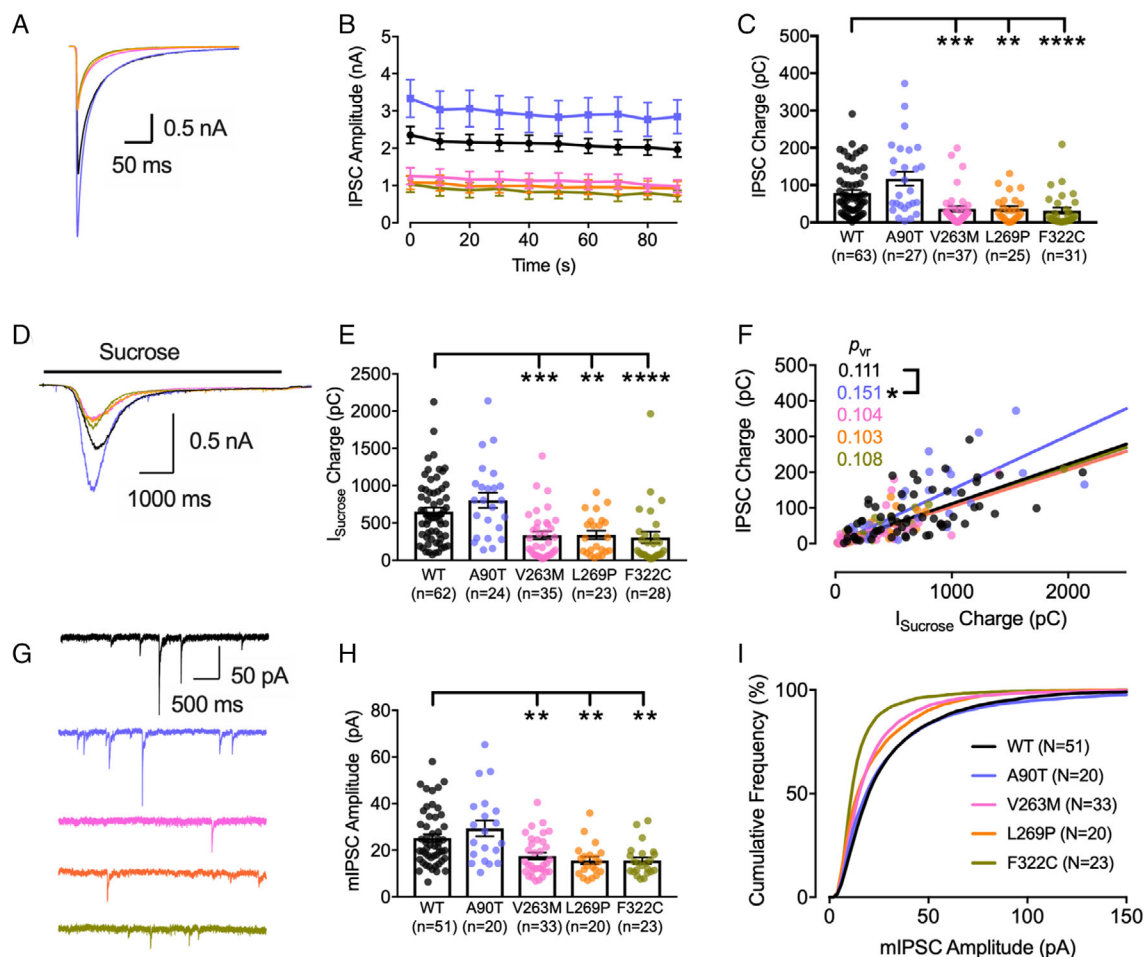


**FIGURE 2:** GABAergic inhibitory postsynaptic currents (IPSCs) and miniature IPSCs (mIPSCs) in striatal neurons. (A) Example traces of single evoked IPSCs from autaptic striatal *Slc32a1*<sup>KO</sup> neurons with lentiviral expression of vesicular gamma-aminobutyric acid transporter (VGAT)<sup>WT</sup> (black), VGAT<sup>A90T</sup> (blue), VGAT<sup>V263M</sup> (pink), VGAT<sup>L269P</sup> (orange), or VGAT<sup>F322C</sup> (green). (B) VGAT<sup>V263M</sup>-, VGAT<sup>L269P</sup>-, and VGAT<sup>F322C</sup>-expressing neurons stimulated at 10-s intervals show reduced IPSC amplitude and (C) reduced IPSC charge. (D) Averaged traces during the application of 0.5 M sucrose, which releases all fusion-competent SVs. (E) Reduced  $I_{\text{sucrose}}$  in neurons expressing VGAT<sup>V263M</sup>, VGAT<sup>L269P</sup>, or VGAT<sup>F322C</sup>. (F) Average vesicular release probability  $\bar{p}_{vr}$ , obtained by linear regression analysis of IPSC charge versus  $I_{\text{sucrose}}$  charge, is significantly higher for VGAT<sup>A90T</sup>. (G) Example traces of mIPSCs, representing fusion events of single synaptic vesicles. (H) Average mIPSC amplitudes are significantly reduced in neurons expressing VGAT<sup>V263M</sup>, VGAT<sup>L269P</sup>, or VGAT<sup>F322C</sup>. (I) Cumulative plot of mIPSC amplitudes. Graphs C, E, and H show values from individual neurons as dots and the mean values as bars with standard error of the mean as error bars. Statistical test applied was Kruskal–Wallis with post-hoc Dunn’s correction for multiple comparisons. Graph F shows data from individual cells as dots and regression lines with an intercept forced to zero. The  $p$  values for comparing slopes were obtained by fitting the data with a linear model, and were adjusted for multiple comparisons using Tukey’s method. (\* $p \leq 0.05$ , \*\* $p \leq 0.01$ , \*\*\* $p \leq 0.001$ , \*\*\*\* $p \leq 0.0001$ ).

region, where the p.(Ala91Thr) variant is located. Because we hypothesized that this variant may disrupt protein–protein interactions, and/or trafficking of VGAT,<sup>34</sup> we chose to introduce this and all other variants into lentiviral expression constructs of the murine VGAT cDNA, rather than work with human VGAT in mouse neurons. The p.(Ala91Thr) variant corresponds to VGAT<sup>A90T</sup> in mice, whereas the amino acid positions of all other variants are conserved. We produced lentiviral particles, which express VGAT and EGFP from separate promoters. Expression of full-length VGAT protein was

confirmed by western blotting of infected striatal *Slc32a1*<sup>KO</sup> neurons in mass culture (Fig. S1). We first evaluated the effects on GABAergic neurotransmission in the absence of endogenous wild-type (WT) VGAT protein, by analyzing to what degree each variant was able to restore GABAergic neurotransmission to mouse VGAT knockout (*Slc32a1*<sup>KO</sup>) neurons. Without rescue by exogenous VGAT expression, the majority of inhibitory *Slc32a1*<sup>KO</sup> neurons are synaptically completely silent and the remainder show only residual neurotransmission.<sup>2</sup> For electrophysiological recordings, we infected

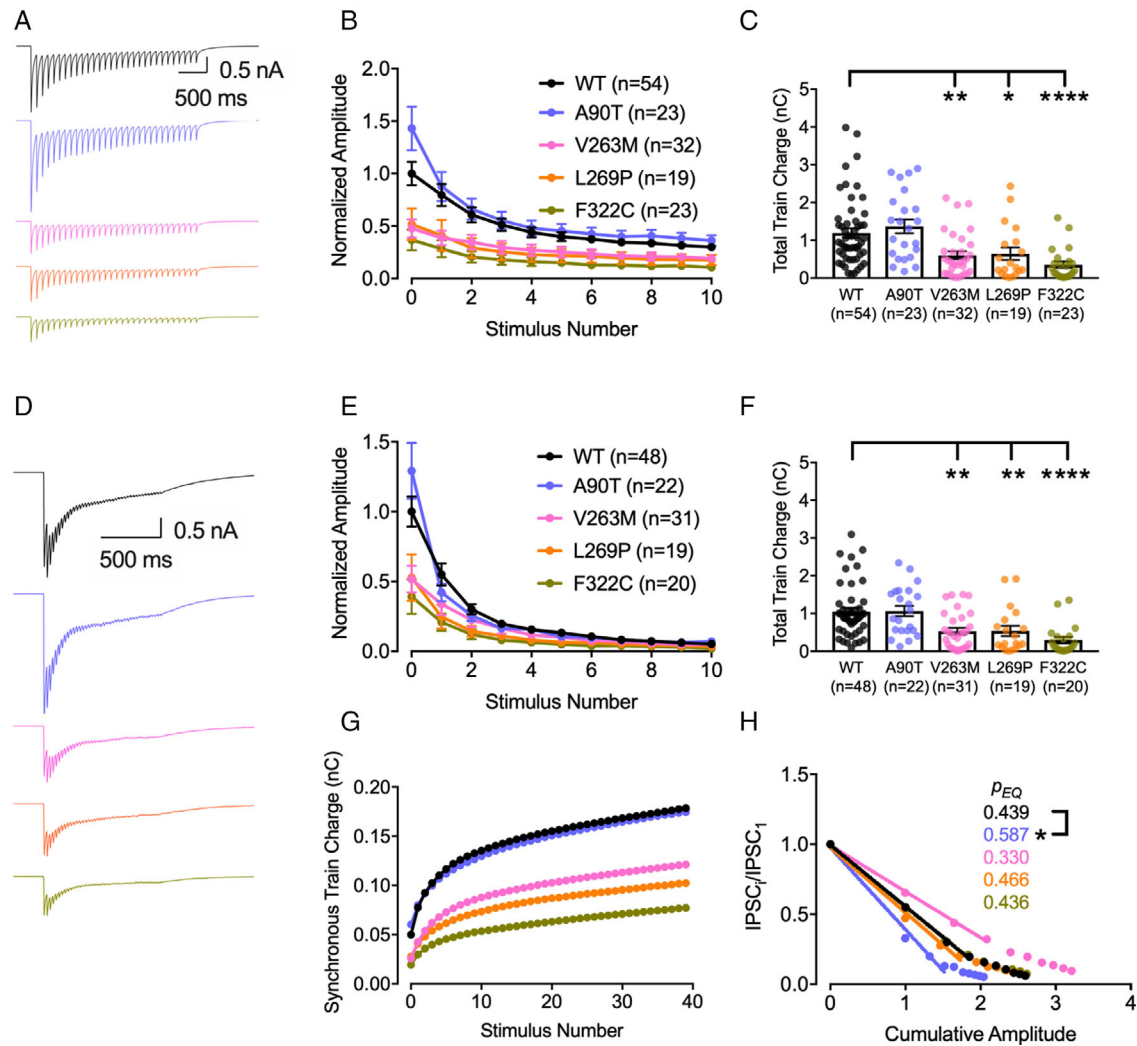


**FIGURE 3:** Stimulation with high-frequency action potential trains – vesicular gamma-aminobutyric acid transporter (VGAT)<sup>A90T</sup> – affects short-term plasticity. (A) Averaged traces obtained during stimulation at 10 Hz from autaptic striatal *Slc32a1*<sup>KO</sup> neurons with lentiviral expression of VGAT<sup>WT</sup> (black), VGAT<sup>A90T</sup> (blue), VGAT<sup>V263M</sup> (pink), VGAT<sup>L269P</sup> (orange), or VGAT<sup>F322C</sup> (green). (B) Reduced inhibitory postsynaptic current (IPSC) amplitudes at 10 Hz in neurons expressing VGAT<sup>A90T</sup>, VGAT<sup>V263M</sup>, VGAT<sup>L269P</sup>, or VGAT<sup>F322C</sup>. Neurons expressing VGAT<sup>A90T</sup> show stronger depression of the second amplitude. (C) Total charge of the GABAergic postsynaptic current during the 10-Hz train is reduced for VGAT<sup>V263M</sup>, VGAT<sup>L269P</sup>, and VGAT<sup>F322C</sup>. (D) Averaged traces obtained during stimulation at 40 Hz. (E) Reduced IPSC amplitudes at 40 Hz in neurons expressing VGAT<sup>V263M</sup>, VGAT<sup>L269P</sup>, and VGAT<sup>F322C</sup>. Neurons expressing VGAT<sup>A90T</sup> showed stronger depression of the second amplitude. (F) Total charge of the GABAergic postsynaptic current during the 40-Hz train is reduced for VGAT<sup>V263M</sup>, VGAT<sup>L269P</sup>, and VGAT<sup>F322C</sup>. (G) Cumulative synchronous IPSC charge of the 40 Hz train. (H) Normalized Elmqvist–Quastel (EQ) plot of the first 10 responses to the 40 Hz train. A line fit through the first four data points reveals that the release probability early in the train,  $p_{EQ}$ , deviates from VGAT<sup>WT</sup> for both VGAT<sup>A90T</sup> and VGAT<sup>V263M</sup>, albeit in opposite directions. The difference in  $p_{EQ}$  is statistically significant for VGAT<sup>A90T</sup>. Graphs C and F show values from individual neurons as dots, and the mean values as bars with standard error of the mean as error bars. The statistical test applied was Kruskal-Wallis with post-hoc Dunn's correction for multiple comparisons. Graph H shows mean values and regression lines fitted to the initial four data points. The  $p$  values for comparing slopes were obtained from pairwise  $t$  tests and adjusted for multiple comparisons using Bonferroni's method. (\* $p \leq 0.05$ , \*\* $p \leq 0.01$ , \*\*\*\* $p \leq 0.0001$ ).

autaptic striatal cultures of *Slc32a1*<sup>KO</sup> neurons on DIV 2–3. Infected neurons were identified based on EGFP expression, and phenotypic rescue of GABAergic neurotransmission in *Slc32a1*<sup>KO</sup> neurons was assessed between DIV 9–14 by patch-clamp recordings in whole-cell voltage clamp configuration.

### Reduced Evoked GABAergic Neurotransmission in Neurons Expressing VGAT<sup>V263M</sup>, VGAT<sup>L269P</sup>, or VGAT<sup>F322C</sup>

We first assayed basal synaptic strength of GABAergic autapses by recording single action potential (AP)-evoked inhibitory postsynaptic currents (IPSCs) at an interstimulus

interval of 10 s. IPSCs were elicited by 1-ms step depolarizations, which produce single escaping APs that trigger  $\text{Ca}^{2+}$ -dependent SV exocytosis. *Slc32a1*<sup>KO</sup> neurons expressing VGAT<sup>V263M</sup>, VGAT<sup>L269P</sup>, or VGAT<sup>F322C</sup>, generated strongly reduced IPSCs when compared with *Slc32a1*<sup>KO</sup> neurons rescued with WT VGAT (VGAT<sup>WT</sup>; Fig. 2A–C). IPSC amplitude (Fig. 2B) and IPSC charge (Fig. 2C) were significantly smaller for these three variants. IPSCs in neurons expressing VGAT<sup>A90T</sup>, in contrast, tended to be

slightly larger than VGAT<sup>WT</sup> IPSCs, although the difference was statistically not significant (Fig. 2A–C, Table 3). Total cell capacitance, which is a measure of cell size and complexity of dendritic arborization, was not affected by expression of any of the variants (Table 3), indicating that growth and differentiation of neurons was unaffected.

Single AP-induced IPSCs typically consume only a small fraction of fusion-competent SVs. To estimate the maximum inhibitory synaptic strength; that is, the

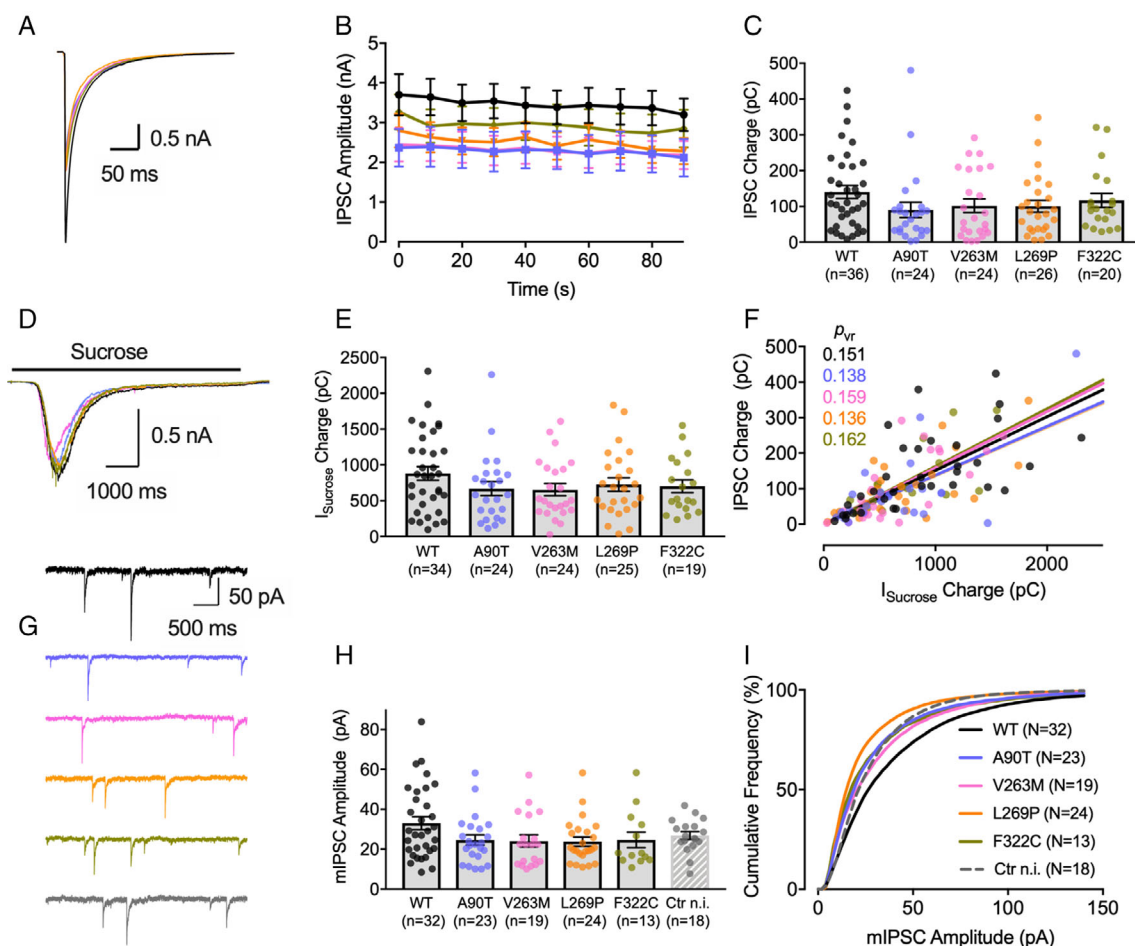


**FIGURE 4: GABAergic inhibitory postsynaptic currents (IPSCs) and miniature IPSCs (mIPSCs) in the presence of endogenous vesicular gamma-aminobutyric acid transporter (VGAT).** (A) Example traces of initial, evoked inhibitory postsynaptic currents (IPSCs) from autaptic striatal *Slc32a1*<sup>WT</sup> and *Slc32a1*<sup>Het</sup> (*Slc32a1*<sup>WT/Het</sup>) neurons with lentiviral expression of VGAT<sup>WT</sup> (black), VGAT<sup>A90T</sup> (blue), VGAT<sup>V263M</sup> (pink), VGAT<sup>L269P</sup> (orange), or VGAT<sup>F322C</sup> (green). (B) Average IPSC amplitudes at 0.1 Hz tend to be smaller for *Slc32a1*<sup>WT/Het</sup> neurons expressing additional VGAT<sup>A90T</sup>, VGAT<sup>V263M</sup>, VGAT<sup>L269P</sup>, or VGAT<sup>F322C</sup>, but are not significantly reduced compared with neurons expressing VGAT<sup>WT</sup>. (C) IPSC charge is not significantly altered in *Slc32a1*<sup>WT/Het</sup> neurons expressing any of the VGAT variants. (D) Averaged traces during the application of 0.5 M sucrose, which triggers release of all fusion-competent SVs. (E)  $I_{\text{sucrose}}$  is not significantly changed by any of the variants in the presence of endogenous VGAT. (F) Average vesicular release probability  $\bar{p}_{\text{vr}}$ , based on the linear fit of IPSC charge versus  $I_{\text{sucrose}}$  charge, was not affected. (G) Example traces of mIPSCs, representing the release of single synaptic vesicles. Uninfected *Slc32a1*<sup>WT</sup> and *Slc32a1*<sup>Het</sup> neurons (Ctr n.i.) are shown in gray. (H) Average mIPSC amplitudes are not significantly reduced in neurons expressing VGAT<sup>A90T</sup>, VGAT<sup>V263M</sup>, VGAT<sup>L269P</sup>, or VGAT<sup>F322C</sup> in addition to endogenous VGAT, although they tend to be smaller than mIPSC amplitudes in neurons expressing additional VGAT<sup>WT</sup>. (I) The cumulative mIPSC amplitude histogram shows a shift toward larger amplitudes for neurons expressing additional VGAT<sup>WT</sup>. Graphs C, E, and H show values from individual neurons as dots, and the mean values as bars with standard error of the mean as error bars. Statistical test applied was Kruskal–Wallis with post-hoc Dunn’s correction for multiple comparisons. Graph F shows data from individual cells as dots and regression lines with an intercept forced to zero. The  $p$  values for comparing slopes were obtained by fitting the data with a linear model and were adjusted for multiple comparisons using Tukey’s method.

product of the total number of readily releasable SVs and quantal size, GABA release was elicited by bath application of 0.5 M sucrose solution for 7 s (Fig. 2D,E). Such hypertonic stimuli generate transient postsynaptic current responses ( $I_{\text{sucrose}}$ ) reflecting exocytosis of all fusion-competent SVs in a  $\text{Ca}^{2+}$ -independent manner.  $I_{\text{sucrose}}$ , therefore, represents an estimate of the maximum synaptic inhibition achievable during high-frequency AP bursts, which lead to rapid consumption of nearly all fusion-competent SVs. Compared with *Slc32a1*<sup>KO</sup> neurons expressing VGAT<sup>WT</sup>,  $I_{\text{sucrose}}$  was significantly reduced in neurons expressing VGAT<sup>V263M</sup>, VGAT<sup>L269P</sup>, or VGAT<sup>F322C</sup>, but not in neurons expressing VGAT<sup>A90T</sup> (Fig. 2E, Table 3). We then estimated the average vesicular release probability  $\bar{p}_{vr}$  representing the fraction of fusion-competent SVs released during single APs, by fitting regression lines to scatter plots of IPSC charge versus  $I_{\text{sucrose}}$  charge (Fig. 2F). Surprisingly,  $\bar{p}_{vr}$  was significantly elevated in *Slc32a1*<sup>KO</sup> neurons expressing VGAT<sup>A90T</sup>, but very similar to VGAT<sup>WT</sup> in neurons expressing VGAT<sup>V263M</sup>, VGAT<sup>L269P</sup>, or VGAT<sup>F322C</sup> (Fig. 2F, Table 3).

### Reduced Quantal Size in Neurons Expressing VGAT<sup>V263M</sup>, VGAT<sup>L269P</sup>, or VGAT<sup>F322C</sup>

To assess whether the reduction in evoked GABAergic neurotransmission can be attributed to reduced vesicular GABA content, we next evaluated the quantal size by measuring amplitudes of miniature inhibitory postsynaptic currents (mIPSCs), which correspond to the spontaneous fusion of single SVs (Fig. 2G-I). Because mIPSC frequency was generally low in resting neurons of striatal autaptic cultures, we recorded mIPSCs during the recovery periods after brief 10-Hz stimulation (30 APs, see below). During repetitive AP firing, presynaptic intracellular  $\text{Ca}^{2+}$  transiently rises, thereby increasing the rate of asynchronous or delayed SV fusion events. The mIPSC amplitude distribution in *Slc32a1*<sup>KO</sup> neurons expressing VGAT<sup>A90T</sup> was indistinguishable from that of neurons expressing VGAT<sup>WT</sup> (Fig. 2I). By contrast, cumulative probability plots of mIPSC amplitudes showed a marked left shift for VGAT<sup>V263M</sup>-, VGAT<sup>L269P</sup>-, and VGAT<sup>F322C</sup>-expressing neurons, indicating a general reduction in mIPSC size (Fig. 2I). Accordingly, average mIPSC amplitudes were significantly reduced for these three variants, (Fig. 2H,I, Table 3, and Fig. S2), which is consistent with less GABA being loaded into SVs carrying these transporter variants. *Slc32a1*<sup>KO</sup> neurons expressing VGAT<sup>V263M</sup>, VGAT<sup>L269P</sup>, or VGAT<sup>F322C</sup> not only showed reduced mIPSC size, but their average mIPSC frequencies also tended to be lower (Table 3). Because partially filled and even empty SVs are known to fuse,<sup>31</sup> an

unknown fraction of very small mIPSCs, representing fusion of partially filled SVs, may escape detection. Therefore, the average quantal size measured in VGAT<sup>V263M</sup>-, VGAT<sup>L269P</sup>-, and VGAT<sup>F322C</sup>-expressing neurons is likely an overestimate. Furthermore, undetected SV fusion events are likely to at least partially account for the reduced mIPSC frequencies observed in neurons expressing VGAT<sup>V263M</sup>, VGAT<sup>L269P</sup>, or VGAT<sup>F322C</sup> (Table 3).

Immediately after stimulus trains, mIPSC frequencies were strongly elevated, sometimes leading to partial overlap and temporal summation of individual events, which not only impairs automatic mIPSC detection through template matching, but also complicates the analysis of mIPSC kinetics. We therefore additionally recorded mIPSCs under conditions of slightly elevated bath osmolarity (50 mM sucrose), which increased the average rate of spontaneously occurring mIPSCs relative to resting conditions, but resulted in fewer overlapping events compared with mIPSC recordings immediately after AP firing. Analysis of the kinetic properties of mIPSCs recorded under conditions of elevated bath osmolarity revealed significantly slower rise times for VGAT<sup>V263M</sup>, VGAT<sup>L269P</sup>, and VGAT<sup>F322C</sup> (Table 3), consistent with a lower peak concentration of GABA being released into the synaptic cleft. Decay time constants were not significantly different from VGAT<sup>WT</sup>, although they tended to be slower for VGAT<sup>V263M</sup>, VGAT<sup>L269P</sup>, and VGAT<sup>F322C</sup>, which might be due to the less favorable signal-to-noise ratio of the smaller mIPSCs recorded in these cells as compared with *Slc32a1*<sup>KO</sup> neurons expressing VGAT<sup>WT</sup> or VGAT<sup>A90T</sup>. In summary, GABAergic neurons expressing VGAT<sup>V263M</sup>, VGAT<sup>L269P</sup>, or VGAT<sup>F322C</sup> show reduced mIPSC quantal size, which is consistent with lower vesicular GABA content, whereas this was not the case for VGAT<sup>A90T</sup>.

### Altered Short-Term Plasticity in Neurons Expressing VGAT<sup>A90T</sup> or VGAT<sup>V263M</sup>

Thus far, we had assayed synaptic strength in response to single presynaptic APs. Because inhibitory synapses in intact circuits are typically activated by AP bursts, we recorded synaptic responses elicited by short AP trains to evaluate how well *Slc32a1*<sup>KO</sup> neurons expressing VGAT<sup>A90T</sup>, VGAT<sup>V263M</sup>, VGAT<sup>L269P</sup>, or VGAT<sup>F322C</sup> can sustain inhibitory neurotransmission at higher AP firing rates in *Slc32a1*<sup>KO</sup> neurons (Fig. 3). Repetitive stimulation at 10 Hz (Fig. 3A-C) and 40 Hz (Fig. 3D-H) leads to a gradual decline of IPSC amplitudes (Fig. 3B,E). In addition to the synchronous IPSCs, postsynaptic responses also consisted of an asynchronous release component, most likely triggered by the sustained elevation in intracellular presynaptic [ $\text{Ca}^{2+}$ ].<sup>35,36</sup> The total IPSC train

charge (IPSC integral over 4.25 s for 10 Hz and over 2.25 s for 40 Hz) representing the sum of synchronous and asynchronous GABAergic neurotransmission was significantly reduced for VGAT<sup>V263M</sup>, VGAT<sup>L269P</sup>, and VGAT<sup>F322C</sup>, but similar to VGAT<sup>WT</sup> for neurons expressing VGAT<sup>A90T</sup> (Fig. 3C,F). To test whether synchronous and asynchronous release are similarly affected by the VGAT variants, we obtained an estimate for the number of synchronously released quanta ( $m_i$ ) by each train stimulus  $i$  by the amplitude ratio  $IPSC_i/mIPSC$  and plotted the synchronous IPSC train charge ( $m_i \times q$ ) in Fig. 3G. For a comparison of synchronous IPSC waveforms with that of total IPSCs, we convolved trains of impulse responses scaled by  $m_i$  with the respective mIPSC waveforms (Fig. S3). Both types of analysis (Fig. 3G, Fig. S3) indicate that the relative contribution of synchronous and asynchronous GABA release to the total IPSCs was unaffected by any of the VGAT variants.

Remarkably, *Slc32a1*<sup>KO</sup> neurons expressing VGAT<sup>A90T</sup> showed an altered short-term plasticity in response to 10 Hz and 40 Hz stimulus trains. Consistent with their higher  $\bar{p}_{vr}$  (Fig. 2F; Table 3), neurons expressing VGAT<sup>A90T</sup> showed larger initial IPSCs and more rapid synaptic depression in response to 10 Hz and 40 Hz stimulus trains (Fig. 3B,E). Elevated  $\bar{p}_{vr}$  is expected to cause faster consumption of fusion-competent SVs during AP trains, resulting in more rapid synaptic depression, whereas neurons with low  $\bar{p}_{vr}$  may show facilitation; that is, a transient enhancement of amplitudes. Among cultured VGAT<sup>WT</sup>-expressing *Slc32a1*<sup>KO</sup> neurons, cells showing either only IPSC depression or transient IPSC facilitation were both observed. By contrast, *Slc32a1*<sup>KO</sup> neurons expressing VGAT<sup>A90T</sup> rarely showed IPSC facilitation. Average IPSC waveforms for all cells analyzed are shown in Fig. 3A and Fig. 3D. To corroborate elevated  $\bar{p}_{vr}$  in neurons expressing VGAT<sup>A90T</sup>, we plotted the amplitude decrement during the first four IPSCs ( $IPSC_n$ ) measured during 40 Hz trains versus the cumulative amplitude of all previous IPSCs ( $\sum_{i=1}^{n-1} IPSC_i$ ) (Fig. 3H).<sup>37</sup>

Under conditions of negligible SV pool replenishment during interstimulus intervals, the negative slope of such plots represents a measure of release probability ( $p_{EQ}$ ).<sup>38</sup> In contrast to the  $\bar{p}_{vr}$ , estimated by the linear fit of IPSC charge vs  $I_{sucrose}$  charge (Fig. 2F),  $p_{EQ}$  is dominated by SVs fusing early during IPSC trains and may therefore be slightly higher if release probability is not homogeneous among all fusion-competent SVs.<sup>39</sup>  $p_{EQ}$  was significantly higher for VGAT<sup>A90T</sup>-expressing cells than for cells expressing VGAT<sup>WT</sup> or any of the other variants (Fig. 3H, Table 3). Surprisingly, the slope of the line fit

also deviated for *Slc32a1*<sup>KO</sup> neurons expressing VGAT<sup>V263M</sup> compared with those expressing VGAT<sup>WT</sup>, albeit in the opposite direction, indicating a lower  $p_{EQ}$  for *Slc32a1*<sup>KO</sup> neurons expressing VGAT<sup>V263M</sup> (Fig. 3H, Table 3), even though their  $\bar{p}_{vr}$  was unaltered when compared with neurons expressing VGAT<sup>WT</sup> (Fig. 2F, Table 3).

### No Dominant-Negative Effects on GABAergic Neurotransmission in the Presence of Endogenous VGAT

Thus far, we had investigated the intrinsic properties of each VGAT variant in *Slc32a1*<sup>KO</sup> neurons; that is, in the absence of endogenous VGAT. However, as all patients are heterozygous for their respective variant, we wanted to assess if any of the variants might exert a dominant-negative effect in the presence of a *Slc32a1*<sup>WT</sup> allele. As co-infection with multiple viruses is inefficient, we decided to infect neuronal cultures from embryos either heterozygous (*Slc32a1*<sup>Het</sup>) or homozygous for the endogenous VGAT allele (*Slc32a1*<sup>WT</sup>). As no obvious differences were detected between these two genotypes upon lentiviral expression of the VGAT variants, we pooled the data obtained in WT and Het cultures (*Slc32a1*<sup>WT/Het</sup>). In the presence of endogenous VGAT, additional lentiviral expression of VGAT<sup>WT</sup>, or any of the variants (VGAT<sup>A90T</sup>, VGAT<sup>V263M</sup>, VGAT<sup>L269P</sup>, VGAT<sup>F322C</sup>) did not cause any differences in basic GABAergic neurotransmission that were statistically significant (Fig. 4 and Table 4). Although we observed a tendency toward smaller IPSC amplitudes (Fig. 4A, B) and IPSC charge (Fig. 4C) for all four VGAT variants compared with *Slc32a1*<sup>WT/Het</sup> neurons infected with VGAT<sup>WT</sup>-encoding lentivirus, we suspected that this may be due to the fact that overexpression of vesicular transporters can increase quantal size beyond what is observed in uninfected control cells.<sup>31,40,41</sup> We therefore included uninfected *Slc32a1*<sup>WT/Het</sup> control neurons (Ctr n.i.) in our analysis of mIPSC amplitudes (Fig. 4G–I). Average quantal size was not significantly different for any of the variants and similar to uninfected control neurons, whereas neurons expressing VGAT<sup>WT</sup> tended to have slightly larger mIPSC amplitudes (Fig. 4H). The cumulative mIPSC amplitude distribution (Fig. 4I) and mIPSC amplitude histogram (Fig. S4) of VGAT<sup>WT</sup>-expressing neurons were shifted toward larger amplitudes in comparison with all four VGAT variants, and also compared with uninfected control neurons. Taken together, these findings indicate that VGAT<sup>A90T</sup>, VGAT<sup>V263M</sup>, VGAT<sup>L269P</sup>, and VGAT<sup>F322C</sup> are less effective at boosting quantal size than VGAT<sup>WT</sup> when expressed in the presence of the *Slc32a1*<sup>WT</sup> allele, but do not exert a dominant-negative effect.

An unexpected result in this set of experiments is that in the presence of endogenous VGAT, VGAT<sup>A90T</sup> appeared to perform more similarly to the other variants with respect to IPSC amplitude, IPSC charge,  $I_{\text{succrose}}$  charge, and quantal size. As VGAT<sup>A90T</sup> was able to rescue quantal size as effectively as VGAT<sup>WT</sup> when expressed in KO neurons (Fig. 2H,I), we would have expected VGAT<sup>A90T</sup> to be able to boost quantal size in the presence of endogenous VGAT. This, however, was not the case (Fig. 4H, I), which indicates, that VGAT<sup>A90T</sup> may perform slightly differently in the presence of VGAT<sup>WT</sup> than in its absence.

## Discussion

In the present study we describe in detail four individuals with a novel developmental and epileptic encephalopathy that harbor de novo missense variants in *SLC32A1*. Reduced GABAergic neurotransmission due to impaired SV loading is the likely cause of the developmental and the epilepsy phenotype in three of the affected individuals, and we provide evidence that effects on synaptic short-term plasticity may be involved in the fourth individual. Both individuals with neonatal seizure onset initially presented with focal and/or impaired-awareness seizures, whereas both individuals with seizure onset at 15–18 months predominantly had generalized tonic-clonic seizures. As all four individuals showed periods of slowed development and even regression with seizure exacerbation and regained lost skills after seizure control improved, the phenotypic description of an *SLC32A1*-related developmental and epileptic encephalopathy is warranted. Additionally, all four individuals experienced longer periods of seizure freedom during the course of epilepsy.

According to data from gnomAD, *SLC32A1* is a gene with a reduced number of missense variants in controls, indicating a selective constraint on this type of variant in a control population that is not affected by severe, early-onset phenotypes, such as epilepsy, DD, and ID (z score for missense variants = 2.3, observed/expected ratio = 0.63).<sup>14</sup> De novo occurrence, and strong in silico and functional data support the causality of variants in individuals 2, 3, and 4 that are located in the transporter domain and cause reduced GABAergic neurotransmission, consistent with impaired SV filling. In individual 1, trio exome sequencing revealed a second de novo missense variant in *CACNA1H*, which was deemed non-causative, as a recent review revealed that evidence for the causal role of *CACNA1H* in monogenic epilepsy is very limited.<sup>42</sup> Compared with the other three, the evidence for causality of the de novo variant in *SLC32A1* in individual 1 is less

compelling, but the functional deficits in synaptic short-term plasticity identified in cultured *Slc32a1*<sup>KO</sup> neurons expressing the N-terminal variant VGAT<sup>A90T</sup> were quite striking, and constitute a likely pathomechanism. As GABAergic neurons often signal through high-frequency AP bursts,<sup>43</sup> stronger synaptic depression may affect signal processing at individual connections, as well as in neuronal circuits.

Although it may seem surprising that alterations in short-term plasticity and deficits in SV filling can lead to similar clinical phenotypes, both functional deficits may similarly reduce synaptic inhibition for certain activity patterns, and thereby exert comparable effects at the circuit and network level. Furthermore, we did in fact also see alterations in release probability in neurons expressing one of the other variants, VGAT<sup>V263M</sup>, when estimated from early synaptic depression during 40-Hz trains. Distinct effects on  $p$  and therefore synaptic short-term plasticity have previously been demonstrated for the vesicular glutamate transporters, VGLUT1 and VGLUT2. In the case of VGLUT1, lower  $p$  was shown to be due to an interaction between VGLUT1 and endophilin A1, a regulator of endocytosis.<sup>44</sup> The VGAT N-terminus contains several motifs that could be involved in endocytic sorting and activity-dependent recycling, and alanine 91 (alanine 90 in mouse) lies adjacent to a polyproline motif of unknown function.<sup>34</sup> However, as VGAT<sup>A90T</sup> effectively rescued quantal size in *Slc32a1*<sup>KO</sup> neurons, this variant appears to be correctly sorted to SVs, at least in the absence of an *Slc32a1*<sup>WT</sup> allele. Nevertheless, variants in the N-terminal domain could potentially affect  $p$  by interfering with VGAT or SV recycling or with other SV properties. Interestingly, Heron et al.<sup>5</sup> also described an N-terminal VGAT variant, p.Gly43Cys, which is in fact located within an SV targeting motif identified by Santos et al.<sup>34</sup>

Within the VGAT transport domain, the location of the variants predicted to affect substrate transport that we identify in the present study are clearly distinct from most variants reported previously by Heron et al.<sup>5</sup> in affected individuals with GEFS+ and familial epilepsy, which are located more distal to the substrate transport domain (Fig. 1, Fig. S5). This difference may explain why the latter group of variants resulted in a milder phenotypic presentation of the affected individuals, especially without DD/ID. A pronounced deficit in VGAT transporter function could potentially even influence trophic actions of GABA early in development, or the developmental shift of GABAergic neurotransmission from excitation to inhibition during nervous system maturation.<sup>45–47</sup> The amino acid, valine, at position 263 is the only position where multiple variants were found in affected individuals.

Interestingly, the aforementioned alteration of the cavity size with the GABA substrate at its bottom is smaller for the previously reported variant p.(Val263Ala)<sup>5</sup> compared with the variant p.(Val263Met) identified in the present study. This, as well as the apparent effect on *p* seen in our study, could potentially explain the distinct and more severe phenotypic effects observed for this variant, whereas the affected individuals identified by Heron et al.<sup>5</sup> did not show DD/ID.

We did not find evidence for altered pain tolerance in the affected individuals in our cohort – a symptom that might point toward disrupted glycinergic or also GABAergic transmission due to the impaired transport capacity of VGAT in neurons of the spinal cord. Enhanced pain responses have been reported for mice heterozygous for VGAT; however, these mice do not show spontaneous seizures or major behavioral deficits.<sup>3</sup> This may indicate that humans and mice differ in their sensitivity to reduced GABAergic and glycinergic neurotransmission, or could also be due to the fact that removal of one allele is not necessarily the functional equivalent of expression of a variant allele. There is very little expression of VGAT outside the nervous system, and we did not identify any prominent non-neurological symptoms in the affected individuals in our cohort.<sup>48</sup>

GABAergic neurotransmission has long been known to play a causal role in epileptic phenotypes, as variants in a variety of GABA receptor subunits were shown to be causal, especially de novo variants in early onset developmental and epileptic encephalopathy.<sup>4,49</sup> The phenotype of the patients in the present study is in line with what is known about disrupted GABA receptor function caused by de novo variants. The wide phenotypic variability ranging from milder epilepsy syndromes, such as a GEFS+ phenotype and familial epilepsies, to the severe end of the spectrum with the phenotype of developmental and epileptic encephalopathy, has also been shown to be caused by disrupted GABA receptor function; for example, due to variants in *GABRA1*, *GABRG2*, or *GABRB3*.<sup>49–51</sup>

In summary, the present findings establish de novo missense variants in *SLC32A1* as a cause of a developmental and epileptic encephalopathy that adds to the description of neurogenetic disorders associated with impaired GABAergic transmission.

### Description of supplemental data

Supplemental.pdf-file contains Supplemental case reports, two Supplemental Tables and four Supplemental Figures.

Supplemental Excel-file contains the completed standard questionnaires with clinical data.

### Acknowledgments

We thank the families for their participation and support of this study. We also thank JeongSeop Rhee and ChungKu Lee for generously providing astrocyte cultures, and Astrid Zeuch for excellent technical assistance. Open Access funding enabled and organized by Projekt DEAL.

### Author Contributions

K.P., R. A.J., and S.M.W. contributed to the conception and design of the study. K.P., H.S., C.B., M.G., E.M.P., G.L.G., F.B., L.B.H., J.R.L., H.T., R.A.J., and S.M.W. contributed to the acquisition and analysis of the data. K.P., J.R.L., H.T., N.B., R.A.J., and S.M.W. contributed to drafting the text or preparing the figures.

### Potential Conflicts of Interest

Lindsay B. Henderson is an employee of GeneDx, Inc. The other authors have nothing to report.

### Data Availability

All data in the project are contained in the manuscript and its supplement. Further information can be provided upon reasonable request.

### References

- Schiöth HB, Roshanbin S, Hägglund MGA, Fredriksson R. Evolutionary origin of amino acid transporter families SLC32, SLC36 and SLC38 and physiological, pathological and therapeutic aspects. *Mol Aspects Med* 2013;34:571–585.
- Wojcik SM, Katsurabayashi S, Guillemin I, et al. A shared vesicular carrier allows synaptic corelease of GABA and glycine. *Neuron* 2006; 50:575–587.
- Yamada MH, Nishikawa K, Kubo K, et al. Impaired glycinergic synaptic transmission and enhanced inflammatory pain in mice with reduced expression of vesicular GABA transporter (VGAT). *Mol Pharmacol* 2012;81:610–619.
- Maljevic S, Møller RS, Reid CA, et al. Spectrum of GABAA receptor variants in epilepsy. *Curr Opin Neurol* 2019;32:183–190.
- Heron SE, Regan BM, Harris RV, et al. Association of SLC32A1 missense variants with genetic epilepsy with febrile seizures plus. *Neurology* 2021;96:e2251–e2260.
- Sobreira N, Schiettecatte F, Valle D, Hamosh A. GeneMatcher: a matching tool for connecting investigators with an interest in the same gene. *Hum Mutat* 2015;36:928–930.
- Cooper GM, Stone EA, Asimenos G, et al. Distribution and intensity of constraint in mammalian genomic sequence. *Genome Res* 2005; 15:901–913.
- Adzhubei I, Jordan DM, Sunyaev SR. Predicting functional effect of human missense mutations using PolyPhen-2. *Curr Protoc Hum Genet* 2013; Jan; 07:Unit7.20;76.
- Jagadeesh KA, Wenger AM, Berger MJ, et al. M-CAP eliminates a majority of variants of uncertain significance in clinical exomes at high sensitivity. *Nat Genet* 2016;48:1581–1586.

10. Schwarz JM, Rödelberger C, Schuelke M, Seelow D. MutationTaster evaluates disease-causing potential of sequence alterations. *Nat Methods* 2010;7:575–576.
11. Ioannidis NM, Rothstein JH, Pejaver V, et al. REVEL: An ensemble method for predicting the pathogenicity of rare missense variants. *Am J Hum Genet* 2016;99:877–885.
12. Kircher M, Witten DM, Jain P, et al. A general framework for estimating the relative pathogenicity of human genetic variants. *Nat Genet* 2014;46:310–315.
13. Wang Y, Lichter-Konecki U, Anyane-Yeboah K, et al. A mutation abolishing the ZMPSTE24 cleavage site in prelamin A causes a progeroid disorder. *J Cell Sci* 2016;129:1975–1980.
14. Karczewski KJ, Francioli LC, Tiao G, et al. The mutational constraint spectrum quantified from variation in 141,456 humans. *Nature* 2020;581:434–443.
15. Zimmermann L, Stephens A, Nam S-Z, et al. A completely Reimplemented MPI bioinformatics toolkit with a new HHpred server at its Core. *J Mol Biol* 2018;430:2237–2243.
16. Webb B, Sali A. Protein structure modeling with MODELLER. *Methods Mol Biol* 2021;2199:239–255.
17. Lei H-T, Ma J, Sanchez Martinez S, Gonen T. Crystal structure of arginine-bound lysosomal transporter SLC38A9 in the cytosol-open state. *Nat Struct Mol Biol* 2018;25:522–527.
18. Baugh EH, Simmons-Edler R, Müller CL, et al. Robust classification of protein variation using structural modelling and large-scale data integration. *Nucleic Acids Res* 2016;44:2501–2513.
19. Ittisoponpisan S, Islam SA, Khanna T, et al. Can predicted protein 3D structures provide reliable insights into whether missense variants are disease associated? *J Mol Biol* 2019;431:2197–2212.
20. Humphrey W, Dalke A, Schulten K. VMD: visual molecular dynamics. *J Mol Graph* 1996;14:27–28.
21. Sayle RA, Milner-White EJ. RASMOL: biomolecular graphics for all. *Trends Biochem Sci* 1995;20:374–376.
22. Trimbuch T, Xu J, Flaherty D, et al. Re-examining how complexin inhibits neurotransmitter release. *Elife* 2014;3:e02391.
23. Hsia H-E, Kumar R, Luca R, et al. Ubiquitin E3 ligase Nedd4-1 acts as a downstream target of PI3K/PTEN-mTORC1 signaling to promote neurite growth. *Proc Natl Acad Sci U S A* 2014;111:13205–13210.
24. Naldini L, Blömer U, Gally P, et al. In vivo gene delivery and stable transduction of nondividing cells by a lentiviral vector. *Science* 1996;272:263–267.
25. Burgalossi A, Jung S, Man KM, et al. Analysis of neurotransmitter release mechanisms by photolysis of caged Ca<sup>2+</sup> in an autaptic neuron culture system. *Nat Protoc* 2012;7:1351–1365.
26. Bekkers JM, Stevens CF. Excitatory and inhibitory autaptic currents in isolated hippocampal neurons maintained in cell culture. *Proc Natl Acad Sci U S A* 1991;88:7834–7838.
27. Mennerick S, Que J, Benz A, Zorumski CF. Passive and synaptic properties of hippocampal neurons grown in microcultures and in mass cultures. *J Neurophysiol* 1995;73:320–332.
28. Clements JD, Bekkers JM. Detection of spontaneous synaptic events with an optimally scaled template. *Biophys J* 1997;73:220–229.
29. Dvornik AC, Hinkley DV, Schechtman E. Efficient bootstrap simulation. *Biometrika* 1986;73:555–566.
30. Gleason JR. Algorithms for balanced bootstrap simulations. *The American Statistician* 1988;42:263–266.
31. Wojcik SM, Rhee JS, Herzog E, et al. An essential role for vesicular glutamate transporter 1 (VGLUT1) in postnatal development and control of quantal size. *Proc Natl Acad Sci U S A* 2004;101:7158–7163.
32. Lipstein N, Verhoeven-Duif NM, Michelassi FE, et al. Synaptic UNC13A protein variant causes increased neurotransmission and dyskinetic movement disorder. *J Clin Invest* 2017;127:1005–1018.
33. Augustin I, Rosenmund C, Südhof TC, Brose N. Munc13-1 is essential for fusion competence of glutamatergic synaptic vesicles. *Nature* 1999;400:457–461.
34. Santos MS, Park CK, Foss SM, et al. Sorting of the vesicular GABA transporter to functional vesicle pools by an atypical dileucine-like motif. *J Neurosci* 2013;33:10634–10646.
35. Kirischuk S, Grantyn R. Intraterminal Ca<sup>2+</sup> concentration and asynchronous transmitter release at single GABAergic boutons in rat collicular cultures. *J Physiol* 2003;548:753–764.
36. Lu T, Trussell LO. Inhibitory transmission mediated by asynchronous transmitter release. *Neuron* 2000;26:683–694.
37. Elmqvist D, Quastel DM. A quantitative study of end-plate potentials in isolated human muscle. *J Physiol* 1965;178:505–529.
38. Neher E. Merits and limitations of vesicle Pool models in view of heterogeneous populations of synaptic vesicles. *Neuron* 2015;87:1131–1142.
39. Taschenberger H, Woehler A, Neher E. Superpriming of synaptic vesicles as a common basis for intersynapse variability and modulation of synaptic strength. *Proc Natl Acad Sci U S A* 2016;113:E4548–E4557.
40. Wilson NR, Kang J, Hueske EV, et al. Presynaptic regulation of quantal size by the vesicular glutamate transporter VGLUT1. *J Neurosci* 2005;25:6221–6234.
41. Daniels RW, Collins CA, Gelfand MV, et al. Increased expression of the drosophila vesicular glutamate transporter leads to excess glutamate release and a compensatory decrease in quantal content. *J Neurosci* 2004;24:10466–10474.
42. Calhoun JD, Huffman AM, Bellinski I, et al. CACNA1H variants are not a cause of monogenic epilepsy. *Hum Mutat* 2020;41:1138–1144.
43. Hu H, Gan J, Gan J, Interneurons JP. Fast-spiking, parvalbumin<sup>+</sup> GABAergic interneurons: from cellular design to microcircuit function. *Science* 2014;345:1255263.
44. Weston MC, Nehring RB, Wojcik SM, Rosenmund C. Interplay between VGLUT isoforms and endophilin A1 regulates neurotransmitter release and short-term plasticity. *Neuron* 2011;69:1147–1159.
45. Ben-Ari Y, Khalilov I, Kahle KT, Cherubini E. The GABA excitatory/inhibitory shift in brain maturation and neurological disorders. *Neuroscientist* 2012;18:467–486.
46. Represa A, Ben-Ari Y. Trophic actions of GABA on neuronal development. *Trends Neurosci* 2005;28:278–283.
47. Lopatina OL, Malinovskaya NA, Komleva YK, et al. Excitation/inhibition imbalance and impaired neurogenesis in neurodevelopmental and neurodegenerative disorders. *Rev Neurosci* 2019;30:807–820.
48. Sundberg BE, Wååg E, Jacobsson JA, et al. The evolutionary history and tissue mapping of amino acid transporters belonging to solute carrier families SLC32, SLC36, and SLC38. *J Mol Neurosci* 2008;35:179–193.
49. Bayat A, Bayat M, Rubboli G, Møller RS. Epilepsy syndromes in the first year of life and usefulness of genetic testing for precision therapy. *Genes (Basel)* 2021;12:1051.
50. Møller RS, Wuttke TV, Helbig I, et al. Mutations in GABRB3: from febrile seizures to epileptic encephalopathies. *Neurology* 2017;88:483–492.
51. Johannessen K, Marini C, Pfeiffer S, et al. Phenotypic spectrum of GABRA1: from generalized epilepsies to severe epileptic encephalopathies. *Neurology* 2016;87:1140–1151.